

Article

Study on Early Shrinkage and Mechanical Properties of Concrete with Various Cementitious Materials

Peng Wang ¹, Ming Xie ^{1,*} and Lei Liu ²¹ College of Civil Engineering, Xijing University, Xi'an 710123, China² Shandong Chunhe New Materials Research Inst. Co., Ltd., Rizhao 276800, China

* Correspondence: 20170223@xijing.edu.cn

Abstract: Due to the rapid development of industrialization, the recycling and utilization of industrial by-products have received extensive attention. In this paper, binary, ternary, and quaternary composite cementitious materials were prepared using steel slag, blast furnace slag, and fly ash, and the effects of different cementitious materials on concrete properties were explored. A variety of solid wastes were mixed, and batches of concrete with high mechanical properties and durability were prepared by adjusting the type and amount of cementitious materials used. A total of 15 batches of concrete were prepared and tested for compressive strength, splitting tensile strength, axial compressive strength, elastic modulus, and drying shrinkage. The test results show that a fly ash, blast furnace slag powder, and steel slag powder ratio of 1:1:2 produces a concrete with the best mechanical properties. Among them, the cube compressive strength can reach 62.9 MPa, the splitting tensile strength is 5.7 MPa, the axial compressive strength and elastic modulus are increased, the early shrinkage is small, the growth rate is slow, and the 28d concrete shrinkage rate is 4.87×10^{-4} . This new type of green mixed concrete can not only control production costs, but can also reduce environmental impact and decrease carbon dioxide emissions.

Keywords: multiple cementitious material systems; compressive strength; elastic modulus; shrinkage; concrete



Citation: Wang, P.; Xie, M.; Liu, L. Study on Early Shrinkage and Mechanical Properties of Concrete with Various Cementitious Materials. *Buildings* **2022**, *12*, 1543. <https://doi.org/10.3390/buildings12101543>

Academic Editors: Cesare Oliviero Rossi, Pietro Calandra, Paolino Caputo, Bagdat Teltayev, Valeria Loise, Michele Porto and Ahmed Senouci

Received: 15 July 2022

Accepted: 19 September 2022

Published: 27 September 2022

Publisher's Note: MDPI stays neutral with regard to jurisdictional claims in published maps and institutional affiliations.



Copyright: © 2022 by the authors. Licensee MDPI, Basel, Switzerland. This article is an open access article distributed under the terms and conditions of the Creative Commons Attribution (CC BY) license (<https://creativecommons.org/licenses/by/4.0/>).

1. Introduction

Steel slag, fly ash, and blast furnace slag powder, as industrial by-products, have been used as cementitious materials in concrete. Taking steel slag as an example, Japan produces 14 million tons of steel slag annually, with a utilization rate of 98.4% [1]. Europe produces 21 million tons a year, with a utilization rate of 87% [2]. According to German standards, 97% of the steel slag is used for road base, earthwork springback and other projects [3]. In the United States, 60.3% of steel slag is used for road base, 10.9% is used for asphalt concrete, 10.8% is used for filler, and 5.0% is used for cement clinker production [4]. In China, the annual output of steel slag exceeds 100 million tons, but the utilization rate is only 29.5%. In 2016, there was still more than 300 million tons of steel slag untreated in China [5]. A large amount of solid waste cannot be eliminated; this waste not only occupies land resources, it also affects the ecological environment [6]. The fine ash collected from flue gas coal combustion is collectively referred to as fly ash. It has the advantages of fine particle size and small porosity, and is widely used in the construction industry [7]. The optimal ratio of fly ash in concrete has long been a topic of interest. Bolomey and Feret equations have been used to calculate that the best efficiency and maximum strength are achieved when the pozzolan/cement ratio is 0.28; however, as that ratio increases, the efficiency gradually decreases [8]. Some scholars have shown through experiments that the optimum content of fly ash is 40%, and that after this value is exceeded, as the content of fly ash continues to increase, the concrete strength begins to decrease. The key factor is the ratio of fly ash to cement [9]. In large engineering structures, to control the temperature rise of concrete, the

amount of fly ash in concrete can usually reach 15% to 50% of the mass of the cementitious material [10]. However the high content of fly ash in concrete has caused some concerns; studies in recent decades have shown that fly ash content of up to 60% can still meet the relevant properties of the required concrete [11]. Concrete properties and engineering properties, including strength development, elastic modulus, and drying shrinkage, are enhanced compared to ordinary silicate concrete [12]. The mechanical strength tests, early self-shrinkage tests and crack resistance tests of concretes with different fly ash contents show that adding a certain amount of fly ash has a positive effect on promoting early crack resistance [13–15]. Additionally, the addition of 20% high calcium fly ash can reduce the aggregate expansion rate, thereby effectively inhibiting the alkali-aggregate reaction of concrete [16]. Test results indicate significant improvement in the strength properties of plain concrete by the inclusion of fly ash as a partial replacement for fine aggregate (sand), which can be effectively used in structural concrete [17]. For self-compacting fly ash concrete, the amount of fly ash has little effect on the early strength of concrete but has a significant effect on the later strength growth rate [18,19]. Blast furnace slag is a by-product of blast furnace ironmaking, and its main chemical composition is similar to that of natural ore. Porous amorphous metastable compounds are obtained by water quenching and rapid cooling treatment, and then blast furnace slag is obtained by grinding. During the water quenching process of blast furnace slag, the heat energy that is not released is stored in the material as chemical energy, making it potentially active and showing high activity under the action of cement hydration or an activator [20,21]. In the field of building materials, blast furnace slag is mainly used in cement admixture, concrete admixture, and road construction. Using blast furnace slag powder to replace 90% of cement, the compressive strength after 28 days is similar to that of conventional concrete, and the elastic modulus, flexural strength, and splitting tensile strength are slightly lower than those of conventional concrete [22]. Blast furnace slag powder not only has a high activity index, but with an increase of the content, the water absorption rate of the concrete increases continuously, and the workability of the cement mortar is improved [23,24]. Mixing blast furnace slag with steel slag in a certain proportion can promote the early hydration of cement, and the active substances in blast furnace slag can weaken the adverse effects of f-CaO and f-MgO in steel slag [25,26]. The 1:1 mixing of blast furnace slag and steel slag in concrete can effectively reduce early hydration heat, prolong the setting time, and improve the strength of concrete [27]. Because the drying shrinkage is related to pore volume, blast furnace slag can improve pore structure by reducing macropores and increasing fine pores. As lead to the capillary pore volume increases, the drying shrinkage gradually becomes larger [28]. Blast furnace slag powder can also improve the durability of concrete, reduce the permeability of chloride ions by 15%, and improve the carbonization resistance of concrete by 3% [29].

Steel slag contains mineral components, such as C_3S and C_2S , which are similar to Portland cement. Steel slag has the characteristics of high density, high strength, and strong wear resistance. After certain treatments, it can be used for road laying cushion and base layer [30]. Studies have shown that under the condition of constant W/B, increasing the content of steel slag will reduce the compressive strength of concrete, increase the permeability of concrete, and reduce the carbonization resistance of concrete [31]. The high replacement rate (10% or 15%) of steel slag powder to cement will lead to a significant decrease in compressive strength during the hydration stage. Replacing the mixture with 4% silica fume (90% cement + 10% steel slag powder) will significantly improve the mechanical properties of the hardened slurry of the mixture (90% cement + 6% steel slag powder + 4% silica fume) [32]. The smaller pores contained in the steel slag promote better water absorption, and the f-CaO and f-MgO in the steel slag are easily hydrolyzed with water, resulting in obvious volume expansion. Because of the poor volume stability of steel slag, proper aging treatment can improve the volume stability [33]. Under high W/B conditions, steel slag accelerates drying shrinkage of concrete. Due to the large porosity of steel slag concrete, the water loss rate is faster. With the continuous increase of steel slag

content, the drying shrinkage of concrete increases gradually [34]. The composite mineral admixture of steel slag powder and blast furnace slag mixed into concrete will greatly improve the performance of concrete, show synergy and mutual activation, and can effectively control the reaction expansion of alkali aggregate and reduce the shrinkage rate by 50% [35]. Using a large amount of steel slag to replace traditional concrete aggregates promotes good mechanical properties, while the high content of calcium and magnesium oxides in hydration limits the concrete durability, even under freeze–thaw conditions. Adding a small amount of air-entraining agent can significantly improve durability [36]. Additionally, steel slag has a strong CO₂ sequestration ability, which can consume expansion components and form carbonized products in a CO₂-rich environment [37].

Steel slag, fly ash, and blast furnace slag composites were studied. At the same water-to-binder ratio, after the composite admixture replaces the cement in the same amount, the anti-carbonation performance and the anti-chloride ion penetration performance of the concrete are significantly improved, and the reaction expansion rate of the alkali aggregate of the concrete is significantly reduced, which can significantly reduce the cementitious material's heat of hydration [38]. The composite use of slag with fly ash, steel slag, and limestone powder can improve the later mechanical properties and chloride ion permeability of concrete, while the composite use of fly ash with steel slag and limestone powder can improve the chloride ion permeability of concrete for 720 days. The composite use of fly ash has the most obvious improvement on the long-term performance of concrete [39]. Using fly ash, steel slag, and blast furnace slag as cementitious materials, the effects on cement hydration mechanical properties and permeability were studied. The results show that the addition of cement containing blast furnace slag and fly ash can reduce the brittleness and improve the long-term strength and resistance to chloride ion penetration of concrete [25]. The effects of steel slag, blast furnace slag, and fly ash on the pore structure of cement paste were studied, and it was found that the mineral admixtures reduced the compressive strength of cement mortar in the early stage and increased it in the later stage. Adding three mineral admixtures can improve the pore structure of cement paste, reduce porosity, and improve pore size distribution [40]. In the development of concrete, the types of mineral components used are constantly changing; solid waste components are now being used as cement replacements to realize a new concept in the green development of concrete. This article discusses the effects of fly ash, slag powder, and steel slag powder on the strength of concrete at different ages. The optimal mix ratio of multicomponent concrete was studied by two methods: single admixture and repeated admixture. High-performance concrete with good durability was prepared, which could not only reduce economic costs, but also reduce CO₂ emissions and greenhouse effects, as well.

2. Materials and Methods

2.1. Raw Materials

Zhong Lian brand P·O 42.5 ordinary Portland cement (C) provided by Rizhao Zhong Lian Port Cement Co., Ltd., (Rizhao, China), was used in this study. The physical properties of the cement are shown in Table 1. All technical performance indicators conformed to the GB175-2007 Chinese standard [41].

Table 1. Physical properties of cement.

| Setting Time (min) | | Desity (g/cm ³) | Fineness (%) | Specific Surface (m ² /kg) | Compressive Strength (MPa) | | | Flexural Strength (MPa) | | |
|----------------------|--------------------|-----------------------------|--------------|---------------------------------------|----------------------------|------|------|-------------------------|-----|-----|
| initial setting time | final setting time | | | | 3d | 7d | 28d | 3d | 7d | 28d |
| 177 | 307 | 3.0 | 8.7 | 372.2 | 23.0 | 38.0 | 47.4 | 5.3 | 5.5 | 6.4 |

In this experiment, fly ash (FA), blast furnace slag powder (GGBS), and steel slag powder (SSP) were used as mineral admixtures. The three mineral admixtures used in the experiment are shown in Figure 1. Fly ash (FA) is produced by Hua Neng Group Lai Wu Power Plant. The physical properties of the fly ash are shown in Table 2.



Figure 1. The three mineral admixtures used in the experiment.

Table 2. Physical properties of the fly ash.

| Water Demand Ratio (%) | Fineness (%) | Loss on Igniting (%) | Activity (%) | | Compressive Strength (MPa) | | Flexural Strength (MPa) | |
|------------------------|--------------|----------------------|--------------|------|----------------------------|------|-------------------------|-----|
| | | | 7d | 28d | 7d | 28d | 7d | 28d |
| 96 | 3.6 | 1.2 | 58.0 | 98.6 | 22.3 | 46.8 | 5.8 | 6.6 |

The blast furnace slag powder (GGBS) is produced by Jinan Lu Xin New Building Materials Co., Ltd. (Jinan, China) The physical properties of the blast furnace slag powder are shown in Table 3.

Table 3. Physical properties of the blast furnace slag powder.

| Density (g/cm ³) | Fineness (%) | Specific Surface (m ² /kg) | Activity (%) | | Compressive Strength (MPa) | | Flexural Strength (MPa) | |
|------------------------------|--------------|---------------------------------------|--------------|------|----------------------------|------|-------------------------|-----|
| | | | 7d | 28d | 7d | 28d | 7d | 28d |
| 2.9 | 0.6 | 421.2 | 77.3 | 92.0 | 29.4 | 43.7 | 6.4 | 7.7 |

Steel slag powder (SSP) is produced by Wuhan Iron and Steel Group. The physical properties of the steel slag powder are shown in Table 4.

Table 4. Physical properties of the steel slag powder.

| Density (g/cm ³) | Fineness (%) | Specific Surface (m ² /kg) | Activity (%) | | Compressive Strength (MPa) | | Flexural Strength (MPa) | |
|------------------------------|--------------|---------------------------------------|--------------|------|----------------------------|------|-------------------------|-----|
| | | | 7d | 28d | 7d | 28d | 7d | 28d |
| 3.1 | 19.3 | 470 | 43.7 | 53.6 | 16.6 | 25.4 | 3.9 | 6.1 |

Natural sand produced in Weifang, Shandong province was used for the experiment. The dust content, apparent density, bulk density, and tight density of the natural sand were 3.9%, 2580 kg/m³, 1330 kg/m³, and 1460 kg/m³. Sieve analysis of the natural sand is shown in Figure 2.

The test uses crushed stone produced in Rizhao, Shandong Province. The elongated and flaky particle content and crushing value index of the crushed stone were 7.4% and 16.5%. The apparent density, bulk density, and tight density of the crushed stone were 2720 kg/m³, 1400 kg/m³, and 1550 kg/m³. The sieving residual percentage of the crushed stone is shown in Table 5.

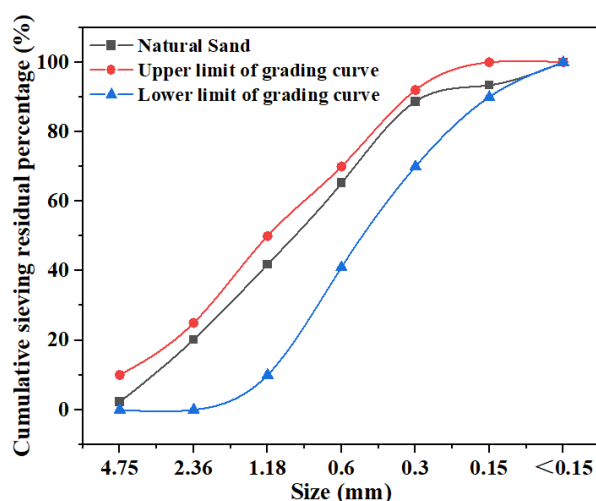


Figure 2. Sieve analysis of the natural sand.

Table 5. Sieving residual percentage of the crushed stone.

| | Square Hole Sieve Side Length (mm) | Cumulative Sieving Residual Percentage (%) | Test Value (%) |
|------------------|------------------------------------|--|----------------|
| Sieving Analysis | 37.5 | - | 0 |
| | 31.5 | - | 0 |
| | 26.5 | 0 | 0 |
| | 19.0 | 0–10 | 8 |
| | 16.0 | - | 54 |
| | 9.50 | 40–80 | 75 |
| | 4.75 | 90–100 | 99 |
| | 2.36 | 95–100 | 100 |

All technical performance indicators of the natural sand and crushed stone conformed to the JGJ52-2006 Chinese standard [42]. The test adopts PCA-I polycarboxylate superplasticizer with a water-reducing rate of 29% manufactured by China Jiangsu Su Bote New Materials Co., Ltd., (Nanjing, China), for regulating the flow of concrete. The density, air content, and bleeding rate of polycarboxylate superplasticizer are $1.054\text{g}/\text{cm}^3$, 3.4%, and 38%. The dosage of polycarboxylate superplasticizer was 1.4% by the mass ratio of all binder materials. The water/binder ratio in this study was 0.4. The fly ash, mineral powder, and steel slag powder used in the test are mixed into concrete according to a certain proportion. The design of the test mix ratio refers to the JGJ/T 233-2011 Chinese standard [43].

2.2. Experimental Design

The total amount of all mineral admixtures remains the same. The experiment was carried out as follows. The experimental design is shown in Figure 3. The mix proportion is shown in Table 6.

First, testing group FA was prepared by replacing part of the cement with 10%, 20%, and 30% fly ash, exploring the early shrinkage and mechanical properties of concrete with a single mineral admixture. Next, testing group GGBS was prepared based on C70F30; the amount of cement was kept unchanged. Blast furnace slag powder in amounts totaling 10%, 15%, and 20% of the mixture were added to replace fly ash. The early shrinkage and mechanical properties of fly ash and blast furnace slag powder concrete were studied. Finally, the experimental group SSP was prepared based on C70F15G15; the cement content of 70% was kept unchanged. The blending ratio of fly ash and blast furnace slag powder was set to 1:1. Steel slag powder was added in amounts equal to a 100%, 75%, 50%, and 25%

replacement of the fly ash and blast furnace slag powder. Studies were then conducted on the early shrinkage and mechanical properties of the multi-mineral component concretes.

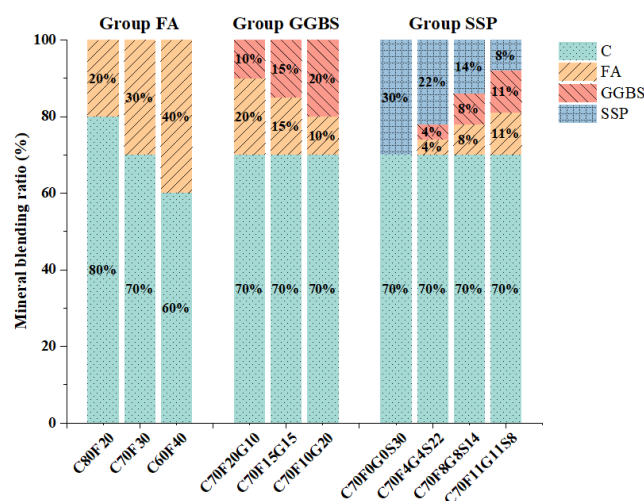


Figure 3. Experimental design.

Table 6. Design of concrete mix per cubic meter (kg).

| Type | Test Number | C | FA | GGBS | SSP | Natural Sand | Crushed Stone | Water | Water Reducer |
|------------|-------------|-------|-------|------|-------|--------------|---------------|-------|---------------|
| Group FA | C80F20 | 340 | 85 | 0 | 0 | 756 | 1042 | 170 | 6.0 |
| | C70F30 | 297.5 | 127.5 | 0 | 0 | 756 | 1042 | 170 | 6.0 |
| | C60F40 | 255 | 170 | 0 | 0 | 756 | 1042 | 170 | 6.0 |
| Group GGBS | C70F20G10 | 297.5 | 85 | 42.5 | 0 | 756 | 1042 | 170 | 6.0 |
| | C70F15G15 | 297.5 | 63.8 | 63.8 | 0 | 756 | 1042 | 170 | 6.0 |
| | C70F10G20 | 297.5 | 42.5 | 85 | 0 | 756 | 1042 | 170 | 6.0 |
| Group SSP | C70F0G0S30 | 297.5 | 0 | 0 | 127.5 | 756 | 1042 | 170 | 6.0 |
| | C70F4G4S22 | 297.5 | 15.9 | 15.9 | 95.6 | 756 | 1042 | 170 | 6.0 |
| | C70F8G8S14 | 297.5 | 31.9 | 31.9 | 63.8 | 756 | 1042 | 170 | 6.0 |
| | C70F11G11S8 | 297.5 | 47.8 | 47.8 | 31.9 | 756 | 1042 | 170 | 6.0 |

To ensure the accuracy of the test, the quality of the mixture in Table 6 is rounded to one decimal place, and the test number is rounded to the nearest whole number.

Group FA, group GGBS, and group SSP all performed early shrinkage and mechanical properties of concrete tests. The mechanical property test process is described in the GB/T 50081-2019 [44] Chinese standard. The early shrinkage test process is described in the GB/T 50082-2009 [45] Chinese standard.

Taking the test number “C70F11G11S8” as an example, C70 refers to the cement content of 70%, F11 refers to the fly ash content of 11%, G11 refers to the mineral powder content of 11%, and S8 refers to the steel slag powder content of 8%.

2.3. Samples Preparation

The specimens of reactive powder concrete were prepared using the following steps.

In this test, a horizontal concrete single-shaft mixer was used for mixing, and the mixing volume of each tray was 45 L. The sand-gravel was dry mixed for 30 s according to the mixing ratio, cement and mineral admixtures were added for dry mixing for 60 s, and high-performance admixtures were added according to the mixing ratio, and the concrete mixture was mixed for 120 s; then, the concrete was allowed to stand for 10 s before being poured into the molds. The specimens were sealed with a plastic cloth and kept in a room environment that had a temperature and relative humidity that was kept at $(20 \pm 2)^\circ\text{C}$ and above 40%, respectively, for 1 day. After curing, the specimens were demolded and moved

to a curing environment with a temperature of $(20 \pm 2) ^\circ\text{C}$ and a relative humidity above 95%, for curing. The curing process is described in the GB/T 50081-2019 Chinese standard.

2.4. Measurement Methods

2.4.1. Early Shrinkage Test

The early shrinkage of concrete is tested by $100 \times 100 \times 515$ mm size. The specimens were taken out from the curing environment at the age of 3 days (calculated by the mixing time of concrete adding water) and placed in a closed environment to determine the initial length, then each group of three specimens were tested for 3 days, 7 days, 14 days, and 28 days concrete shrinkage rate. The average test results are accurate to 0.1%.

2.4.2. Mechanical Property Test

The YAW-300 microcomputer fully-automatic universal tester, provided by Shanghai Hua Long Instrument Equipment Co., Ltd., Shanghai, China, was applied for the determination of the mechanical property test.

1. **Compressive strength** The compressive strength of concrete is tested by $100 \times 100 \times 100$ mm size. After curing for 3 days, 7 days, and 28 days in the curing environment, the specimens are taken out and tested for concrete compressive strength. There are 3 specimens in each group. The average test results are accurate to 0.1 MPa. The test adopts pressure control, and the test is carried out at 0.5 MPa/s.
2. **Splitting tensile strength** The splitting tensile strength of concrete is tested by $100 \times 100 \times 100$ mm size. After curing for 3 days, 7 days, and 28 days in the curing environment, the specimens are taken out and tested for concrete splitting tensile strength. There are 3 specimens in each group. The average test results are accurate to 0.1 MPa. The test adopts pressure control, and the test is carried out at 0.5 MPa/s.
3. **Elastic Modulus** The Elastic Modulus of concrete is tested by $100 \times 100 \times 300$ mm size. After curing for 28 days in the curing environment, the specimens are taken out and tested for concrete elastic modulus. There are three specimens in each group. The average test results are accurate to 0.1GPa. The test adopts pressure control, and the test is carried out at 0.5 MPa/s. First, the initial load of about 0.5 MPa is held for 30 s, the dry scores on both sides are read, it is then loaded to 30% of the axial compressive strength, held for about 30 s, and the thousandths on both sides are read and calculated. The average value of the deformation amount on both sides was calculated. After reading the indication, the concrete is unloaded to 0.5 MPa for 30 s at the same speed and the dial indicators on both sides are read, respectively. The process is repeated three times to determine that the difference between the two sides of the deformation is not more than 15% of the average value. The above procedure is repeated, the fourth loading is performed, and the average value of the elastic modulus is obtained. The early shrinkage and elastic modulus tests of concrete are shown in Figure 4.

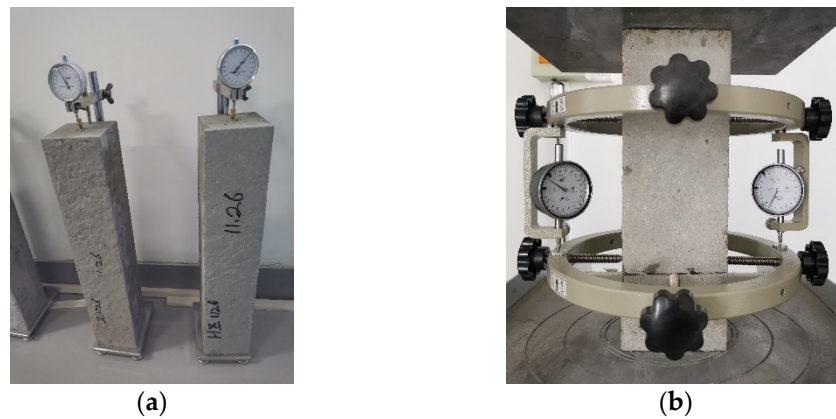


Figure 4. Mechanical test of the concrete part. (a) Concrete early shrinkage test; (b) Concrete elastic modulus test.

3. Results

3.1. Concrete Early Shrinkage Test

Figure 5 is the early shrinkage of concrete.

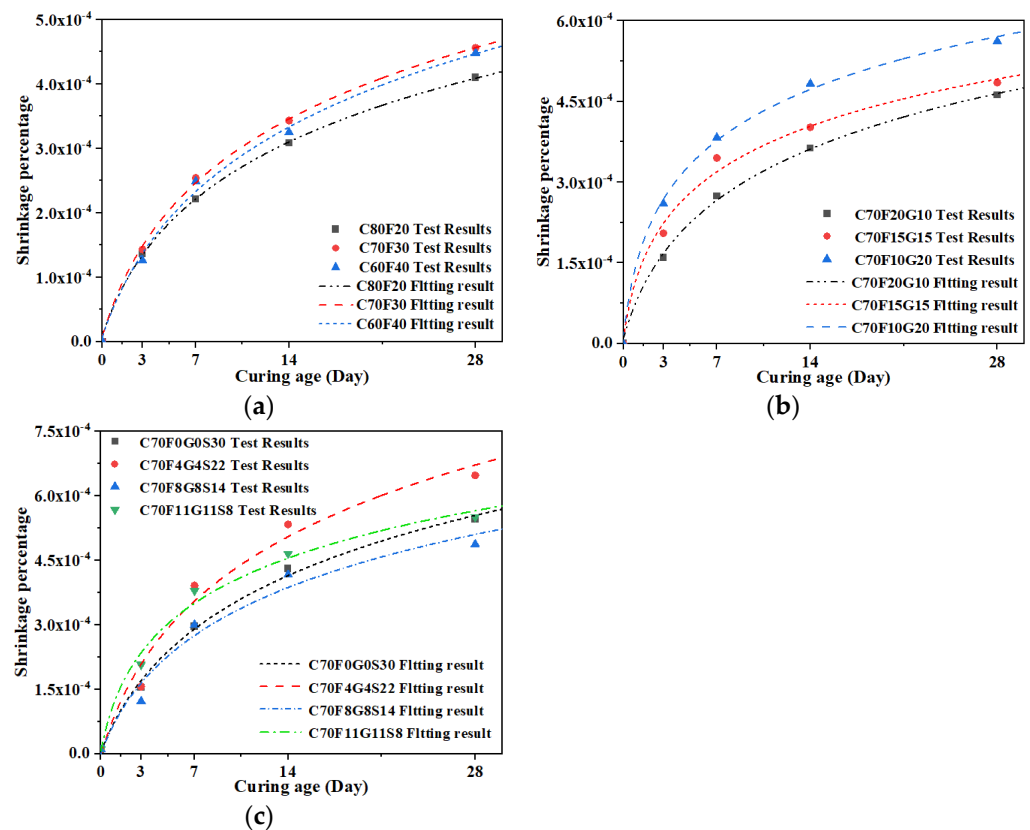


Figure 5. Early shrinkage of concrete. (a) Group FA early shrinkage; (b) Group GGBS early shrinkage; (c) Group SSP early shrinkage.

In group FA, shrinkage at 3 days was essentially the same. At the age of 7 days, the highest shrinkage rate of C70F30 is 2.54×10^{-4} , which is 3.3×10^{-5} and 5.0×10^{-6} larger than that of C80F20 and C60F40. The shrinkage rate of concrete at 14 days has an obvious gradient. The shrinkage rates of C80F20, C70F30, and C60F40 are 3.08×10^{-4} , 3.43×10^{-4} , and 3.25×10^{-4} , respectively. The maximum shrinkage rate of C70F30 in 28 days is 5.09×10^{-4} , which differs from C80F20 and C60F40 by 4.6×10^{-5} , 8×10^{-6} .

In group GGBS, with the increase of mineral powder content, the shrinkage rate of concrete increases gradually. The shrinkage rates of C70F10G20 at 3 days, 7 days, 14 days, and 28 days were 2.6×10^{-4} , 3.83×10^{-4} , 4.83×10^{-4} , and 5.62×10^{-4} , respectively. The shrinkage rate of C70F15G15 is smaller and the shrinkage rate of C70F20G10 is the smallest. The difference between the two is 4.5×10^{-5} , 7.1×10^{-5} , 3.9×10^{-5} , and 2.3×10^{-5} in 3 days, 7 days, 14 days, and 28 days, respectively.

In group SSP, the growth rate of shrinkage rate of C70F4G4S22 reached 150.6% at 7 days of age, which was 58.4%, 4.7%, and 67.5% higher than that of C70F0G0S30, C70F8G8S14, and C70F11G11S8, respectively. At 14 days, the shrinkage rate of C70F4G4S22 was 5.3×10^{-4} , and the difference in shrinkage rate of C70F0G0S30, C70F8G8S14, and C70F11G11S8 was small. At 28 days, the maximum shrinkage rate of C70F4G4S22 is 6.5×10^{-4} , the shrinkage rate of C70F11G11S8 is 5.5×10^{-4} , the shrinkage rate of C70F0G0S30 is 5.4×10^{-4} , and the minimum shrinkage rate of C70F8G8S15 is 4.87×10^{-4} .

The nonlinear curve fitting is performed on the early shrinkage of concrete, and the fitting parameters of the shrinkage change are shown in Table 7.

Table 7. Fitting parameters of concrete early shrinkage curve.

| Equation | Category | Test Number | <i>a</i> | <i>b</i> | <i>c</i> | <i>R</i> ² |
|------------------------|----------|-------------|----------|----------|----------|-----------------------|
| $y = a - b \ln(x + c)$ | FA | C80F20 | −1.44 | −1.62 | 2.60 | 0.9998 |
| | | C70F30 | −1.61 | −1.80 | 2.57 | 0.9983 |
| | | C60F40 | −2.07 | −1.90 | 3.10 | 0.9922 |
| | GGBS | C70F20G10 | −8.84 | −1.63 | 1.81 | 0.9978 |
| | | C70F15G15 | 5.09 | −1.31 | 0.72 | 0.9848 |
| | | C70F10G20 | 8.09 | −1.46 | 0.61 | 0.9969 |
| | | C70F0G0S30 | −2.41 | −2.32 | 2.90 | 0.9926 |
| | SSP | C70F4G4S23 | −2.59 | −2.72 | 2.57 | 0.9600 |
| | | C70F8G8S15 | −1.72 | −2.00 | 2.38 | 0.9513 |
| | | C70F11G11S8 | 1.61 | −1.67 | 1.03 | 0.9791 |

3.2. Concrete Mechanical Properties Test

3.2.1. Compressive Strength

Figure 6 shows the compressive strength of group FA. When the replacement amount of fly ash is more than 30%, the strength decreases with the increase of the content. Among them, the C70-F30 group has higher strength. The 3 days, 7 days, and 28 days cube compressive strengths under standard curing are 30.5 MPa, 45.4 MPa, and 65.7 MPa, respectively. Compared with the 7 days strength growth rate of 48.9%, the 28 days strength growth rate was decreased to 44.7%. By comparing the C80-F20 group and the C60-F40 group, it was found that the fly ash replacement rate increased from 20% to 40%, and the compressive strength of the concrete cubes decreased. The compressive strengths of 3 days and 7 days differ by 6 MPa and 10.8 MPa, respectively, and the strength of 28 days is the same, with a difference of 2.1 MPa. In the C80-F20 group, the 7 days intensity growth rate was 57.6%, and the 28 days intensity growth rate was 32.2%, a decrease of 25.4%. In the C60-F40 group, the 28 days intensity growth rate increased by 18% compared with the 7 days intensity growth rate, and the 7 days and 28 days intensity growth rates were 51.4% and 69.4%, respectively.

As shown in Figure 7, in the GGBS group, with the increase of mineral powder content, the concrete strength gradually increased. Under the standard during 3 days, the strength of the C70F20G10 group and C70F15G15 group is the same as 26 MPa, and the strength of the C70F10G20 group is 30.9 MPa. When the curing age increases, the strength shows an obvious gradient upward trend with the difference in the mineral powder replacement rate. After 7 days of standard curing, the strengths of the C70F20G10 group, C70F15G15 group, and C70F10G20 group were 35.5 MPa, 42.7 MPa, and 48.1 MPa respectively. The strong growth rate of the C70F15G15 group was the largest at 64.2%, which was 27.7%

and 8.5% higher than that of the C70F20G10 group and the C70F10G20 group. Under the standard curing for 28 days, the maximum strength of the C70F10G20 group reached 60.5 MPa, which was 14.5 MPa and 10.8 MPa different from that of the C70F20G10 group and C70F15G15 group, respectively. Compared with the 7 days concrete strength growth rate of 55.7%, the 28 days strength growth rate decreased to 46.6%. The strong growth rate of the C70F20G10 group on 7 days and 28 days increased from 36.5% to 57.7%.

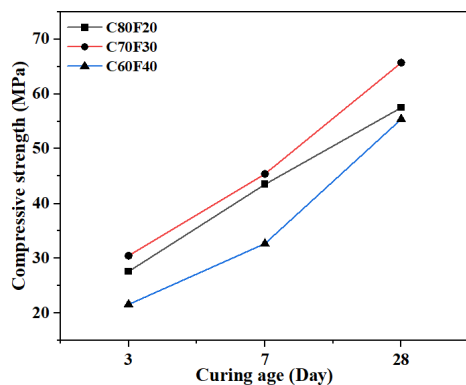


Figure 6. Group FA Compressive Strength.

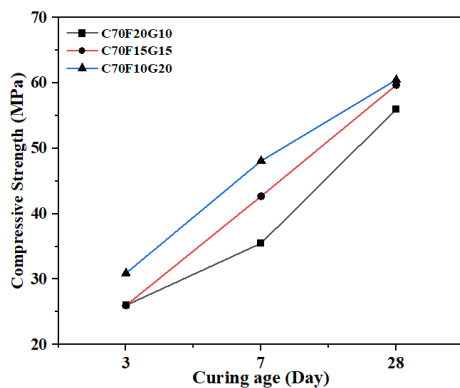


Figure 7. Group GGBS Compressive Strength.

As shown in Figure 8, in the SSP group, when the slag substitution rate is greater than 15%, the strength gradually decreases. Under the standard curing 3 days, the strength is the same, 30.4 MPa, 30.2 MPa, 29.9 MPa, and 28.3 MPa, respectively. After 7 days of standard curing, the strength increased rapidly and formed an obvious gradient. The highest strength of the C70F8G8S14 group reached 62.9 MPa, followed by the C70F11G11S8 group with a strength of 42.8 MPa, and finally the C70F4G4S22 and C70F0G0S30 groups, which were 40.9 MPa and 38.5 MPa, respectively. The strong growth rate of the C70F8G8S14 group was the largest at 54.2%, which was 2.9% higher than that of the C70F11G11S8 group. The strongest growth rates of the C70F0G0S30 and C70F4G4S22 groups were 26.6% and 35.4%, respectively, a difference of 8.8%. The 28 days concrete strength continued to increase, and the C70F8G8S14 group reached a peak value of 62.9 MPa, compared with 7 days, the strongest growth rate decreased to 36.4%. The 28 days compressive strength of the C70F4G4S22 group was 59.2 MPa, which was 3.7 MPa and 6.6 MPa higher than that of the C70F11G11S8 group and C70F0G0S30 group, respectively. The 28 days strength growth rate increased to 44.7%, which was 8.6% and 15.5% bigger than that of the C70F0G0S30 group and C70F11G11S8 group, respectively.

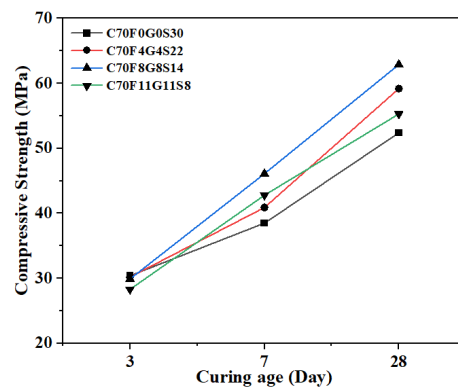


Figure 8. Group SSP Compressive Strength.

3.2.2. Splitting Tensile Strength

Figure 9a shows the Group FA Splitting tensile strength. In group FA, the splitting tensile strength of concrete reaches the maximum when the fly ash content is 30%. The splitting tensile strength of the C70F30 group is much higher than that of the C60F40 group and the C80F20 group, and the 3 days, 7 days, and 28 days strengths are 4.1 MPa, 5.6 MPa, and 7.4 MPa, respectively. The splitting tensile strength of the C60F40 group and C80F20 group is similar, the difference in 3 days strength is 0.3 MPa, the 7 days strength is the same, both are 4.1 MPa, and the 28 days strengths are 5.4 MPa and 5.8 MPa, respectively, with a difference of 0.4 MPa.

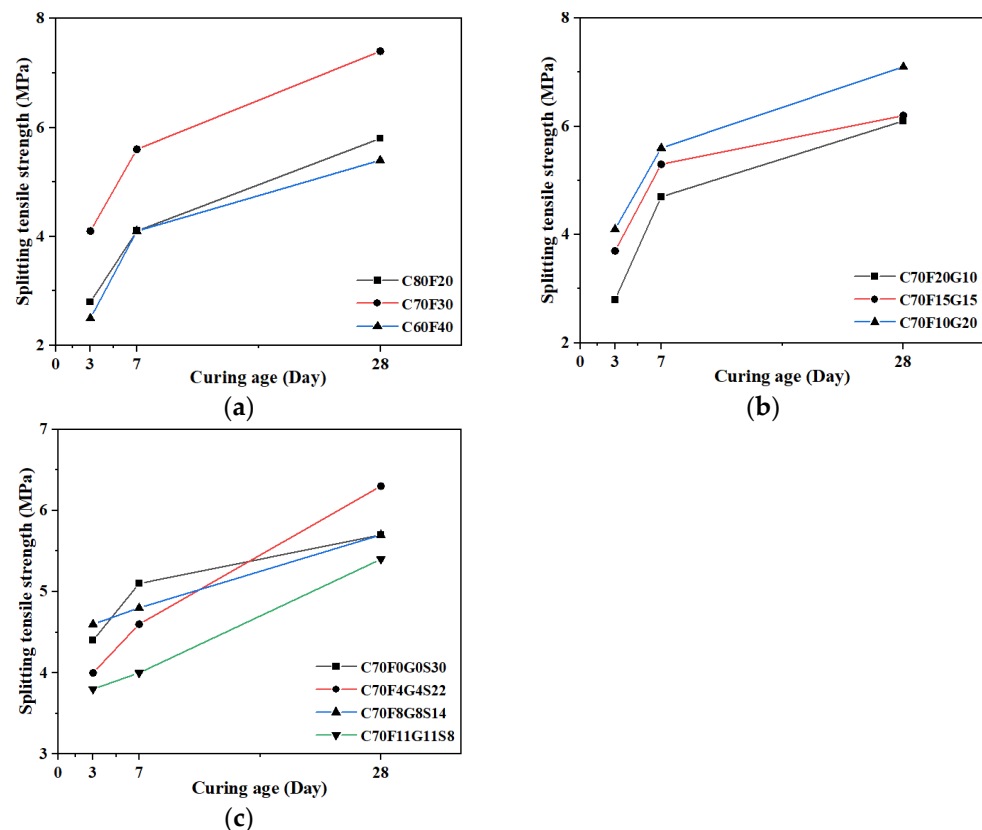


Figure 9. Splitting tensile strength of concrete. (a) Group FA Splitting tensile strength; (b) Group GGBS Splitting tensile strength; (c) Group SSP Splitting tensile strength.

Figure 9b shows the Group GGBS Splitting tensile strength. In group GGBS, with the increase of mineral powder content, the splitting tensile strength increases gradually. The splitting tensile strength of the C70F10G20 group was 4.1 MPa higher than that of

the C70F15G15 group and C70F20G10 group, which were 0.4 MPa and 1.3 MPa higher than those of the C70F15G15 group and C70F20G10 group, respectively, under standard curing for 3 days. For 7 days, the splitting strengths of the C70F10G20 group, C70F15G15 group, and C70F20G10 group were 5.6 MPa, 5.3 MPa, and 4.7 MPa, respectively. At 28 days, the C70F15G15 group and the C70F20G10 group were the same at 6.2 MPa and 6.1 MPa, respectively, and the C70F10G20 group had a maximum of 7.1 MPa.

Figure 9c shows the Group SSP Splitting tensile strength. In group SSP, with the increase of the content of steel slag powder, the splitting tensile strength gradually increased, and the maximum strength reached 6.3 MPa when the content was 22%. The splitting tensile strengths of C70F0G0S30, C70F4G4S22, C70F8G8S14, and C70F11G11S8 were 4.4 MPa, 4.0 MPa, 4.6 MPa, and 3.8 MPa, respectively, under standard curing for 3 days. When curing for 7 days, C70F0G0S30 is 5.1 MPa, C70F4G4S22 is 4.6 MPa, the strength growth rates are 15.9% and 15%, respectively. For C70F8G8S14 and C70F11G11S8, the growth rates are 4.3% and 5.3% slower, and the splitting tensile strengths are 4.8 MPa and 4.0 MPa, respectively. After 28 days of curing, the strength of C70F4G4S22 was 6.3 MPa, and the growth rate reached a maximum of 37%. The strengths of C70F0G0S30, C70F8G8S14, and C70F11G11S8 increased to 5.7 MPa, 5.7 MPa, and 5.4 MPa, respectively. Compared with C70F4G4S22, the growth rate was 25.2%, 18.2%, and 2% different.

3.2.3. Elastic Modulus

Table 8 shows the axial compressive strength and elastic modulus of concrete.

Table 8. Axial compressive strength and elastic modulus of concrete.

| Test Number | Axial Compressive Strength (MPa) | Elastic Modulus (GPa) |
|-------------|----------------------------------|-----------------------|
| C80F20 | 44.6 | 29.1 |
| C70F30 | 50.9 | 29.6 |
| C60F40 | 41.6 | 26.6 |
| C70F20G10 | 44.8 | 27.7 |
| C70F15G15 | 48.8 | 28.5 |
| C70F10G20 | 52.4 | 30.1 |
| C70F0G0S30 | 47.2 | 29.1 |
| C70F4G4S23 | 47.4 | 28.6 |
| C70F8G8S15 | 48.2 | 28.6 |
| C70F11G11S8 | 42.8 | 29.0 |

In group FA, when the content of fly ash reaches 30%, the maximum axial compressive strength of C70F30 is 50.9 MPa, which is 6.3 MPa and 9.3 MPa higher than that of C80F20 and C60F40. The highest elastic modulus of C70F30 is 29.6 GPa, which is 0.5 GPa and 3 GPa different from that of 20% and 40%.

In group GGBS, with the increase of mineral powder content, the elastic modulus gradually increased and reached a peak at 20% mineral powder content. The elastic modulus of C70F10G20 is 30.1 GPa, which is 2.4 GPa higher than that of C70F20G10 and 1.6 GPa higher than that of C70F15G15. The maximum axial compressive strength of C70F10G20 is 52.4 MPa, which is 7.6 MPa and 3.6 MPa higher than that of C70F15G15 and C70F20G10, respectively.

In group SSP, when the mixing ratio of fly ash, mineral powder, and steel slag powder is 1:1:2, the maximum axial compressive strength of C70F8F8S15 is 48.2 MPa, and the elastic modulus is 28.6 GPa. The C70F0F0S30 axial compressive strength is 47.2 MPa, the elastic modulus is 29.1 GPa, which is 0.2 MPa lower than the C70F4F4S22 axial compressive strength, 0.5 GPa higher elastic modulus, 4.4 MPa higher than the C70F11F11S8 axial compressive strength, and 0.1 GPa difference in elastic modulus.

In the concrete axial compression test, due to the insufficient stiffness of the compression tester, when the load exceeds the peak load, the press rapidly releases the accumulated energy, causing the specimen to be destroyed instantaneously, and the curve cannot record

the descending section. Taking C70F10F20 with the highest axial compressive strength as an example, Table 9 shows the peak stress–strain results of axial compressive strength, and Figure 10 shows the stress–strain curve.

Table 9. Axial compressive strength and elastic modulus of concrete.

| Test Number | Peak Strain ε_{\max} | Peak Stress σ_{\max} | Strain at the Limit Point of Elastic Segment ε | Stress at the Limit Point of Elastic Segment σ |
|-------------|----------------------------------|-----------------------------|--|---|
| C70F10G20-1 | 44.08 | 55.97 | 34.59 | 44.78 |
| C70F10G20-2 | 50.63 | 48.58 | 42.78 | 43.56 |
| C70F10G20-3 | 42.38 | 50.38 | 33.43 | 42.44 |

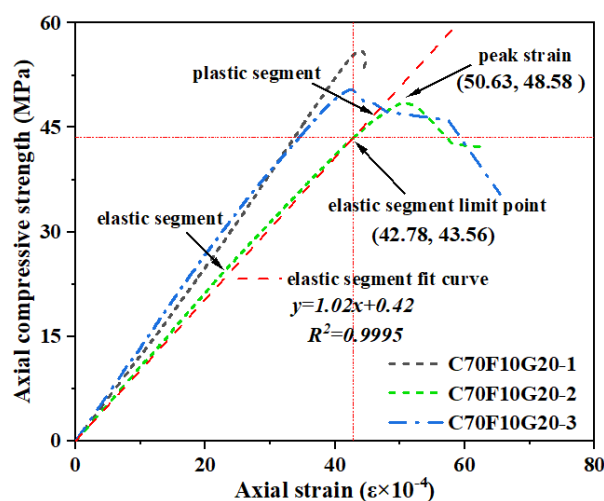


Figure 10. C70F10G20 group concrete stress-strain curve.

In the axial compression test of the concrete specimen, the stress–strain curve can be divided into an ascending section and a descending section, of which the ascending section can be divided into two stages. Take the specimen C70F10G20 as an example:

The first stage of rising is the elastic stage. The stress–strain curve grows almost linearly, and the crack is in a stable period under axial pressure. The aggregate and the matrix are slightly deformed, the microcracks in the bonding interface gradually develop, and new cracks appear in some internal pores. In Figure 10, the elastic limit points (42.78, 43.56) correspond to 0.84 times the peak strain.

The second stage of rising is the plastic stage. After the limit elastic point, the stress–strain curve shows a nonlinear upward curve. As the load continues to increase, the cracks in the concrete continue to develop and extend, and visible cracks appear on the surface of the specimen. When the stress reaches its maximum value, the strain reaches its peak value, corresponding to the peak strain point (50.63, 48.58) in Figure 10.

The third stage is the descending section of the stress–strain curve. With the continuous application of the load, penetration cracks develop on the specimen, forming macroscopic fracture failure, and the interface cracks lead to frictional slippage between the matrix and the aggregate. The load on the specimen is counterbalanced by the frictional resistance on the shear plane and the residual adhesive force, and the residual bearing capacity decreases slowly.

Because concrete is an inhomogeneous material, the failure modes of axial compression are diverse, including shear failure, split failure, surface peeling, local crushing, etc. The failure modes of some specimens are two or more combined failures. Taking C70F10G20 as an example, Figure 11 shows C70F10G20 group concrete axial compression failure.

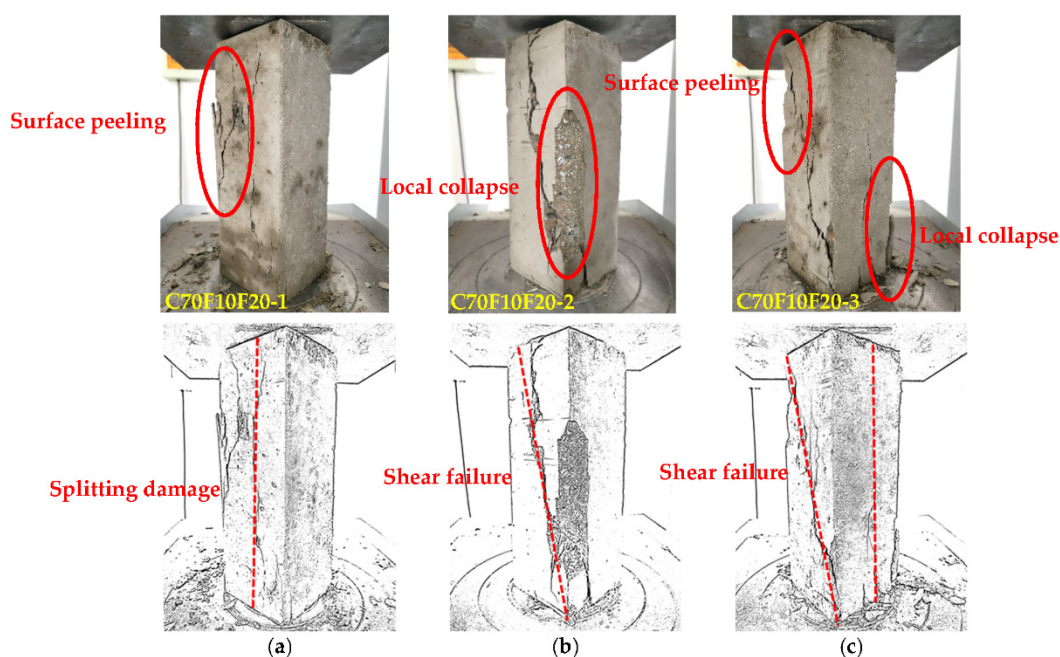


Figure 11. C70F10G20 group concrete axial compression failure. (a) Splitting damage, surface peeling; (b) Shear failure, local collapse; (c) Split failure, shear failure.

4. Discussion

4.1. Effect of Fly Ash on Concrete Mechanics and Shrinkage

It can be seen from Figure 6 that the compressive strength of concrete increases gradually with age when the amount of fly ash remains unchanged. The morphological effect of fly ash and the effect of fly ash microaggregate reduce the strength of concrete mixed with fly ash in the early stage. At the same age, the compressive strength of concrete mixed with fly ash first increases and then decreases with the increase of fly ash content. When the content of fly ash is between 20% and 30%, its effect is more significant. When the content of fly ash is 30%, the compressive strength of concrete reaches a maximum of 65.7 MPa; when the content of fly ash exceeds 30%, the compressive strength gradually decreases. Fly ash can convert the cement hydration product $\text{Ca}(\text{OH})_2$ to C-S-H. As the cement content of the concrete decreases, the hydration products will decrease; therefore, the amount of $\text{Ca}(\text{OH})_2$ and C-S-H generated will decrease, and the compressive strength of the concrete will decrease accordingly [8]. At 28 days, the axial compressive strength of concrete increases firstly with the increase of fly ash content, the peak value reaches 50.9 MPa (30% fly ash content), and then decreases rapidly; when the fly ash content is 40%, the axial compressive strength is 41.6 MPa. The general change trend of the elastic modulus of concrete is the same as that of the axial compressive strength. When the content of fly ash is 30%, its maximum value is 29.6 GPa. The reason is that the microaggregate effect of fly ash fills the voids in the concrete. The active effect accelerates the hydration reaction of concrete, making the overall stiffness of the concrete larger, and the strength and elastic modulus also increase [12].

At 3 days, the hydration rates of concrete with different fly ash contents were the same. With the deepening of cement hydration and the filling effect of fly ash, the compactness of the internal structure of the concrete mixed with fly ash is significantly improved, and the elastic modulus is greatly improved. In the 3-day and 7-day age range, the hydration rate of concrete with different fly ash content is the same, and the shrinkage growth rate shows no significant difference. After 7 days, the fly ash particles participate in the hydration, the volume increases, and the surrounding cement hydration products are squeezed, making the original, relatively loose C-S-H change, improving the compactness of the cement stone-hardened body structure. The fly ash hydration process consumes the cement hydration

product $\text{Ca}(\text{OH})_2$, reduces the content of large particles of $\text{Ca}(\text{OH})_2$ crystals between the aggregate interface and the cement stone, and improves the uniformity and compactness of the interior of the concrete [46,47]. When the content of fly ash exceeds 30%, the filling and compacting effect caused by the “morphological effect” of fly ash particles offsets part of the reduction in the early hydration degree of fly ash. Therefore, when the content of fly ash exceeds 30%, its reducing effect on shrinkage is weakened.

4.2. Effects of Fly Ash and Blast Furnace Slag Powder on Concrete Mechanics and Shrinkage

The compounding of fly ash and mineral powder can improve the strength of concrete. Under the same mixing ratio, with the increase of age, the strength of concrete increases continuously. When slag powder and fly ash are mixed at a 2:1 ratio, the compressive strength of concrete reaches 60.5 MPa. With the continuous increase of the amount of mineral powder, the activity of the concrete continues to increase, and the aggregate reaction continues to increase, which has an obvious effect on the improvement of the early strength. Incorporating an appropriate amount of fly ash and slag powder into the cement can effectively reduce the porosity of the cementitious material system, form good mutual filling between different particles, and can effectively improve the mechanical properties of concrete [48].

Figure 5b reflects the effect of fly ash and slag micro powder on the drying shrinkage of concrete. It can be seen from the figure that as the content of slag micro powder increases, the dry shrinkage value also increases. The shrinkage of concrete in the early stage is relatively large, and then it tends to be stable. This may be caused by the fast hydration rate of slag powder in the early stage, more pores in the cement stone, and faster evaporation of capillary water. In the range of 20% of the content, the dry shrinkage value increases with the increase of the content. This is because the fineness of the slag micropowder is larger than that of the cement particles, which plays the role of particle gradation and has a faster hydration speed, filling the pores in the cement stone [49]. When the dosage is further increased, due to the larger specific surface area of the slag, the amount of surface water in the system increases, thus increasing the amount of drying shrinkage.

4.3. Effects of Various Mineral Admixtures on Concrete Mechanics and Shrinkage

When the content of steel slag powder is 15%, the strength of the concrete is greatly improved, and the compressive strength is 62.9 MPa; but when the content exceeds 15%, the compressive strength is reduced to 55.3 MPa. Steel slag powder contains the same components as cement, C_2S , and C_3S . In the process of concrete hardening, the early hydration activity of steel slag micropowder is relatively high, but when the steel slag powder is finely ground, there are a lot of defects on the particle surface, and the activity has been exerted to a certain extent. When the steel slag powder is matched with fly ash and slag micro powder, the characteristics of the mineral admixture can be well exerted. The early compressive strength of concrete is relatively high, and the later strength development is stable. The f-CaO in the steel slag powder can better stimulate the activity of fly ash and slag micro powder [50].

In the multicomponent cementitious material system, due to the different activities of various mineral components, the early hydration is dominated by mineral powder and steel slag powder, the reaction is severe, the concrete shrinks and deforms greatly, the shrinkage rate increases rapidly, and the fly ash hydration occurs in the later stage. In the secondary hydration reaction, the fly ash hydration rate is slower and the reaction is more thorough. The cementitious material can better fill the internal pores of the concrete, improve the compactness, and reduce the evaporation of free water, thereby reducing the shrinkage and deformation of the concrete. It can be seen from Figure 5c that the shrinkage rate of concrete mixed with steel slag powder is generally larger, and the shrinkage rate becomes larger as the amount of steel slag powder increases. At 8% and 30%, the shrinkage of concrete at 28 days gradually becomes similar. At the age of 28 days, the shrinkage ratio of concrete mixed with 28% steel slag powder is the highest, the shrinkage ratio is 6.47×10^{-4} , and the

shrinkage ratio of concrete mixed with 14% steel slag powder is 4.87×10^{-4} , which is the smallest. This is mainly due to the low activity of the steel slag powder in the early stage; f-CaO and f-MgO did not have an effective shrinkage effect on concrete under the condition of sufficient grinding. Therefore, when steel slag powder, slag micro powder, and fly ash are used in concrete, the workability of the concrete can be improved, the hydration heat release of the cementitious material system can be reduced, and the later strength growth can be larger. At the same time, the $\text{Ca}(\text{OH})_2$ generated by the hydration reaction of the steel slag can stimulate the activity of the slag micro powder. The slag micro powder can eliminate the defects of f-CaO and f-MgO in the steel slag and improve the stability of the concrete improved [51].

4.4. Economic Cost and Carbon Emissions Calculation

In order to analyze the impact of the replacement of parts of cement by steel slag powder, blast furnace slag powder, and fly ash on concrete production costs and environmental benefits, a simple assessment is made. Since there are some differences in the prices of materials in different places, the prices calculated in this section of the economic evaluation are considered with reference to the local prices of the materials selected in this experiment. Table 10 lists the carbon emissions and raw materials cost (based on the data in China) [52].

Table 10. Carbon emission and material cost for each component of blended cement.

| Materials | CO ₂ Emission (kg/kg) | Cost (RMB/ton) |
|-----------|----------------------------------|----------------|
| C | 470 | 0.93 |
| FA | 170 | 0.083 |
| GGBS | 234 | 0.008 |
| SSP | 200 | 0.218 |

Comparing all test groups, it is found that, except for the C60F40 group, the cost of the other test groups is not as low as that of the SSP group. However, the large amount of fly ash in C60F40 is not conducive to the development of concrete early strength and does not meet the requirements of concrete construction. Comparing the CO₂ emissions of the SSP group, we found that when the mixing ratio of fly ash, blast furnace slag powder, and steel slag powder is 1:1:2, the concrete emits lower CO₂, which can reduce the burden of CO₂ production on the environment

5. Conclusions

(1) When the ratio of steel slag, blast furnace slag, and fly ash is 1:2:1, the mechanical properties of concrete prepared by replacing 30% of the cement are better than other ratios. The 28-day compressive strength of concrete was 62.9 MPa and the axial compressive strength was 48.2 MPa, but the splitting tensile strength and static elastic modulus decreased. However, with a gradual increase in the amount of steel slag, the performance of concrete gradually decreased.

(2) Under the same water–binder ratio, the steel slag, blast furnace slag, and fly ash can be tightly packed by adjusting the mixing ratio. After replacing the cement with the same amount of composite mineral admixture, not only is the pore size distribution improved and the gap between the powders reduced, but the shrinkage and deformation of the concrete are reduced, as well. At this time, the minimum drying shrinkage of concrete in 28 days is 4.87×10^{-4} .

(3) Mixing steel slag, blast furnace slag, and fly ash in a certain proportion not only produces concrete with good mechanical properties, it also makes the cost price controllable, significantly reduces carbon dioxide emission, and improves the impact on the environment.

Author Contributions: Conceptualization, P.W. and L.L.; Data curation, P.W.; Formal analysis, P.W.; Investigation, L.L.; Methodology, M.X.; Project administration, L.L.; Resources, M.X.; Supervision, M.X.; Visualization, P.W.; Writing—original draft, P.W.; Writing—review & editing, P.W. All authors have read and agreed to the published version of the manuscript.

Funding: This research was funded by the Natural Science Foundation of Shandong Province of China (No. ZR2021ME002).

Institutional Review Board Statement: Not applicable.

Informed Consent Statement: Not applicable.

Data Availability Statement: The data used to support the findings of this study are available from the corresponding author upon request.

Conflicts of Interest: The authors declare that there are no conflict of interest regarding the publication of this paper.

References

1. NSA. Production and Uses of Steel Slag in Japan. Available online: <http://www.slg-jp/e/statistics/index.html> (accessed on 11 September 2017).
2. Euroslag, Statistics. Available online: <http://www.euroslag.com/products/statistics/2012/> (accessed on 11 September 2017).
3. Motz, H.; Geiseler, J. Products of steel slags an opportunity to save natural resources. *Waste Manag.* **2001**, *21*, 285–293. [CrossRef]
4. Ilyushechkin, A.Y.; Roberts, D.G.; French, D.; Harris, D.J. *IGCC Solids Disposal and Utilisation*; Final Report for ANLEC Project 5-0710-0065; CSRIRO: Canberra, Australia, 2012.
5. Guo, J.; Bao, Y.; Wang, M. Steel slag in China: Treatment, recycling, and management. *Waste Manag.* **2018**, *78*, 318–330. [CrossRef] [PubMed]
6. Shi, C.; Qian, J. High performance cementing materials from industrial slags—A review. *Resour. Conserv. Recycl.* **2000**, *29*, 195–207. [CrossRef]
7. Dunstan, E.R., Jr. *Ash-in-Concrete Model Development*; Final Report (No. EPRI-GS-6129); Electric Power Research Institute: Palo Alto, CA, USA; Dunstan Inc.: Lakewood, CO, USA, 1989.
8. Pekmezci, B.Y.; Akyuz, S. Optimum usage of a natural pozzolan for the maximum compressive strength of concrete. *Cem. Concr. Res.* **2004**, *34*, 2175–2179. [CrossRef]
9. Onera, A.; Akyuz, S.; Yildiza, R. An experimental study on strength development of concrete containing fly ash and optimum usage of fly ash in concrete. *Cem. Concr. Res.* **2005**, *35*, 1165–1171. [CrossRef]
10. Xu, G.; Shi, X.M. Characteristics and applications of fly ash as a sustainable construction material: A state-of-the-art review. *Resour. Conserv. Recycl.* **2018**, *136*, 95–109. [CrossRef]
11. Zhang, D.X.; Li, J.W.; Guo, W.B. Experimental study on the influence of fly ash quality and content on concrete performance. *Contemp. Chem. Ind.* **2021**, *50*, 262–265.
12. Hemalatha, T.; Mapa, M.; George, N.; Sasmal, S. Physico-chemical and mechanical characterization of high volume fly ash incorporated and engineered cement system towards developing greener cement. *J. Clean. Prod.* **2016**, *125*, 268–281. [CrossRef]
13. Xie, W.; Zhang, H.J.; Li, S.S. Basic Mechanical Properties Test of Fly Ash Concrete. *Appl. Mech. Mater.* **2012**, *238*, 138–141. [CrossRef]
14. Khan, I.; Castel, A.; Gilbert, R.I. Effects of Fly Ash on Early-Age Properties and Cracking of Concrete. *Aci. Mater. J.* **2017**, *114*, 673–681. [CrossRef]
15. Riding, K.A.; Poole, J.L.; Schindler, A.K.; Juenger, M.C.G.; Folliard, K.J. Quantification of effects of fly ash type on concrete early-age cracking. *Aci Mater. J.* **2008**, *105*, 149–155.
16. Sun, Y.F.; Li, S.X.; Lu, Y. Experimental study on alkali activity test and inhibition of the alkali-aggregate reaction. *Fly Ash Compr. Util.* **2020**, *34*, 84.
17. McCarthy, M.J.; Dhir, R.K. Development of high volume fly ash cements for use in concrete construction. *Fuel* **2005**, *84*, 1423–1432. [CrossRef]
18. Ponikiewski, T.; Golaszewski, J. The self-compacting properties of the concrete mixture of cement with calcareous fly ash addition. *Cem. Wapno Beton* **2012**, *17*, 233.
19. Skazlic, M.; Roskovic, R.; Pecur, I.B. Properties of self-compacting concrete with high fly-ash content. *Gradevinar* **2008**, *60*, 945–952.
20. Sato, K.; Konishi, E.; Fukaya, K.; Koibuchi, K.; Ishikawa, Y.; Iijima, Y. Properties of blast-furnace slag powder produced by classification process. 1. Hydraulic hardening capacity of high fineness blast-furnace slag powder. *Trans. Iron Steel Inst. Jpn.* **1986**, *26*, 85.
21. Sato, K. Properties of blast-furnace slag powder produced by classification process. 2. Hydraulic hardening capacity of high fineness blast-furnace slag powder. *Trans. Iron Steel Inst. Jpn.* **1985**, *71*, 781.
22. Saafan, M.A.; Etman, Z.A. Microstructure and durability of ground granulated blast furnace slag cement mortars. *Iran. J. Sci. Technol. Trans. Civ. Eng.* **2021**, *45*, 1457–1465. [CrossRef]
23. Gholampour, A.; Ozbakkaloglu, T. Performance of sustainable concretes containing very high volume Class-F fly ash and ground granulated blast furnace slag. *J. Clean. Prod.* **2017**, *162*, 140–1417. [CrossRef]

24. Li, Q.L.; Chen, M.Z.; Liu, F.; Wu, S.P.; Sang, Y. Effect of superfine blast furnace slag powder on properties of cement-based materials. *Mater. Res. Innov.* **2015**, *19*, 168–171. [[CrossRef](#)]
25. Sun, J.W.; Zhang, P. Effects of different composite mineral admixtures on the early hydration and long-term properties of cement-based materials: A comparative study. *Constr. Build. Mater.* **2021**, *294*, 123547. [[CrossRef](#)]
26. He, T.S.; Li, Z.B.; Zhao, S.Y.; Zhao, X.G.; Qu, X.L. Study on the particle morphology, powder characteristics and hydration activity of blast furnace slag prepared by different grinding methods. *Constr. Build. Mater.* **2021**, *270*, 121445. [[CrossRef](#)]
27. Wang, Q.; Yan, P.; Mi, G. Effect of blended steel slag–GBFS mineral admixture on hydration and strength of cement. *Constr. Build. Mater.* **2012**, *35*, 8–14. [[CrossRef](#)]
28. Zhang, W.; Hama, Y.; Na, S.H. Drying shrinkage and microstructure characteristics of mortar incorporating ground granulated blast furnace slag and shrinkage reducing admixture. *Constr. Build. Mater.* **2015**, *93*, 267–277. [[CrossRef](#)]
29. Kim, Y.; Hanif, A.; Usman, M.; Munir, M.J.; Kazmi, S.M.S.; Kim, S. Slag waste incorporation in high early strength concrete as cement replacement: Environmental impact and influence on hydration & durability attributes. *J. Clean. Prod.* **2018**, *172*, 3056–3065.
30. Jiang, Y.; Ling, T.C.; Shi, C.J. Characteristics of steel slags and their use in cement and concrete—A review. *Resour. Conserv. Recycl.* **2018**, *136*, 187–197. [[CrossRef](#)]
31. Wang, Q.; Yan, P.; Yang, J.; Zhang, B. Influence of steel slag on mechanical properties and durability of concrete. *Constr. Build. Mater.* **2013**, *47*, 1414–1420. [[CrossRef](#)]
32. Amin, M.S.; El-Gamal, S.M.A.; Abo-El-Enein, S.A.; El-Hosiny, F.I.; Ramadan, M. Physico-chemical characteristics of blended cement pastes containing electric arc furnace slag with and without silica fume. *HBRC J.* **2015**, *11*, 321–327. [[CrossRef](#)]
33. Gencil, O.; Karadag, O.; Oren, O.H.; Bilir, T. Steel slag and its applications in cement and concrete technology: A review. *Constr. Build. Mater.* **2021**, *283*, 122783. [[CrossRef](#)]
34. Qiang, W.; Mengxiao, S.; Jun, Y. Influence of classified steel slag with particle sizes smaller than 20 μm the properties of cement and concrete. *Constr. Build. Mater.* **2016**, *123*, 601–610. [[CrossRef](#)]
35. Li, Y.F.; Kong, F.Y.; Du, R.Q. Application of high performance concrete mixed with steel slag powder in concrete pavements. In Proceedings of the Ninth International Conference of Chinese Transportation Professionals, Harbin, China, 5–9 August 2009, pp. 1–7.
36. Pellegrino, C.; Gaddo, V. Mechanical and durability characteristics of concrete containing EAF slag as aggregate. *Cem. Concr. Compos.* **2009**, *31*, 663–671. [[CrossRef](#)]
37. Wang, A.G.; He, M.C.; Mo, L.W. Research progress of building materials prepared from the carbonized curing steel slag. *Mater. Rep.* **2019**, *33*, 2939–2948.
38. Yang, Q.; Yang, Q. Effects of Compound Mineral Admixture with Steel Slag on Durability of Concrete. *J. Tongji Univ. Nat. Sci.* **2010**, *38*, 1200–1204.
39. Wang, Z.; Wang, D. Influence of Different Multi-mineral Admixtures on Long Period Performance of Concrete. *Bull. Chin. Ceram. Soc.* **2015**, *34*, 2392–2397.
40. Li, Y.; Chen, Y. Influence of ground mineral Influence of ground mineral admixtures on pore structure of hardened cement paste and strength of cement mortar. *J. Chin. Silic. Soc.* **2006**, *34*, 575–579. [[CrossRef](#)]
41. GB175-2007; Common Portland Cement. The State Bureau of Quality and Technical Supervision: Beijing, China, 2007.
42. JGJ52-2006; Standard for the Quality and Inspection Methods of Sand and Stone for Ordinary Concrete. Ministry of Construction of the People's Republic of China: Beijing, China, 2006.
43. JGJ/T 233-2011; Specification for Mix Proportion Design of Cement Soil. Ministry of Housing and Urban-Rural Development of the People's Republic of China: Beijing, China, 2011.
44. GB/T 50081-2019; Standard for Test Methods of Concrete Physical and Mechanical Properties. The State Bureau of Quality and Technical Supervision: Beijing, China, 2019.
45. GB/T 50082-2009; Standard for Test Methods of Long-Term Performance and Durability of Ordinary Concrete. The State Bureau of Quality and Technical Supervision: Beijing, China, 2009.
46. Chindaprasirt, P.; Jaturapitakkul, C.; Sinsiri, T. Effect of fly ash fineness on microstructure of blended cement paste. *Constr. Build. Mater.* **2007**, *21*, 1534–1541. [[CrossRef](#)]
47. Kwan, A.K.H.; Chen, J.J. Adding fly ash microsphere to improve packing density, flowability and strength of cement paste. *Powder Technol.* **2013**, *234*, 19–25. [[CrossRef](#)]
48. John, S.K.; Nadir, Y.; Girija, K. Effect of source materials, additives on the mechanical properties and durability of fly ash and fly ash-slag geopolymer mortar: A review. *Constr. Build. Mater.* **2021**, *280*, 122443. [[CrossRef](#)]
49. Li, Y.; Bao, J.L.; Guo, Y.L. The relationship between autogenous shrinkage and pore structure of cement paste with mineral admixtures. *Constr. Build. Mater.* **2010**, *24*, 1855–1860. [[CrossRef](#)]
50. Rafat, S. Utilization (recycling) of iron and steel industry by-product (GGBS) in concrete: Strength and durability properties. *J. Mater. Cycles Waste Manag.* **2014**, *16*, 460–467.
51. Khan, M.S.H.; Castel, A.; Akbarnezhad, A.; Foster, S.J.; Smith, M. Utilisation of steel furnace slag coarse aggregate in a low calcium fly ash geopolymer concrete. *Cem. Concr. Res.* **2016**, *89*, 220–229. [[CrossRef](#)]
52. Wu, M.; Zhang, Y.; Ji, Y.; Liu, G.; Liu, C.; She, W.; Sun, W. Reducing environmental impacts and carbon emissions: Study of effects of superfine cement particles on blended cement containing high volume mineral admixtures. *J. Clean. Prod.* **2018**, *196*, 358–369. [[CrossRef](#)]